Impact Response Evaluation of a Restrained Whole Human Body Finite Element Model under Far-side 90 and 60 degree Impacts

Mike W J Arun, Sagar Umale, John R Humm, Narayan Yoganandan, Frank A Pintar

Abstract The objective of the current study was to evaluate the impact response of the Global Human Body Model Consortium (GHBMC) Human Body Model (HBM) by comparing its various response parameters to those obtained from Post-Mortem Human Subjects (PMHS) experiments. In addition, rib fractures predicted by the HBM were also compared with those sustained by the PMHS. The evaluation was performed under two different impact scenarios - lateral (90 degree), and oblique (60 degree). Also simulations were performed with and without pre-tensioning in the seatbelt for each scenario. Experimental contact forces, regional accelerations and displacements were compared to those obtained from simulations for both the scenarios. The correlation between the experimental and simulation data were quantified using correlation analysis (CORA). The rib fractures and corresponding Abbreviated Injury Scale (AIS) score observed in the experiments were compared to that of simulations. The simulations with the pre-tensioned HBM under-predicted the number of fractures that are observed in the PMHS and the HBM predicted fractures were higher in the cases with no pre-tensioning compared to those of with pre-tensioning. In the pre-tensioned case, the HBM under-predicted the head and T1 displacements, whereas, over predicted T12 and sacrum in both the impact cases. The average combined CORA ratings of the accelerations and contact forces for the with and without pre-tensioning cases were 0.7 and 0.56 in the lateral impact, and the ratings were only 0.5 and 0.46 in the oblique impact. In summary, the study recommends further improvement in the biofidelity of the model under oblique loading mode by improving component level biofidelity of the GHBMC model – thoracic and lumbar spine for example.
Keywords Computational modeling, GHBMC, far-side, human body modeling, injury

I. INTRODUCTION

The crashes in which the occupants are seated opposite to the struck side are defined as far side crashes. Each year, significant number of occupants are injured in these crashes [1-6]. In general, injury mechanisms in far-side impacts are thought to be significantly different from near-side impacts. Therefore, occupant protection strategies for far-side crashes must be different from near-side crashes. Traditionally, controlled laboratory tests are used to delineate injury mechanisms to develop counter-measures. To date, however, there are few studies that have investigated biomechanical responses in far-side impact. Forman *et al* [7] tested three male PMHS under repeated lateral (90-deg) far-side impact on a sled with simplified boundary conditions. The study reported an interrelation between D-ring position, arm positions, pre-tensioning, and impact speed. Pintar, Yoganandan [8] tested six restrained PMHS under repeated lateral far-side impact on a sled using a buck with detailed boundary conditions. Shoulder retention effectiveness was analyzed using different belt configurations to reduce head excursion and injuries to the thorax. Because of the paucity of experimental studies in the far-side crashes, computational surrogates like finite element human body models (FE-HBM) could be used to supplement experimental studies.

In an effort to develop a computational surrogate, the FE-HBM that was used in the current study has been developed by the Global Human Body Models Consortium (GHBMC). The GHBMC model (version 4.3) represents 50th percentile American male with a seated posture. The Computer Aided Design (CAD) geometry of the model was constructed using computed tomography (CT), magnetic resonance imaging (MRI), and upright MRI obtained from a representative living volunteer (Age: 26 years, Height: 174.9 cm, and Weight: 78.6 kg). The geometry was split into five body regions: head, neck, thorax, abdomen, and pelvis and lower extremity

Mike W J Arun is an Assistant Professor at the Department of Neurosurgery, Medical College of Wisconsin (MCW), USA (marun@mcw.edu). Sagar Umale is a Post-Doctoral Fellow, John R Humm is a Research Engineer, Narayan Yoganandan and Frank A Pintar are Professors at the Department of Neurosurgery, Medical College of Wisconsin (MCW), USA.

(plex). The geometries were then meshed, validated, and integrated into a whole body finite element model. The integrated whole body finite element model consists of 1.3 million nodes, and 1.9 million elements. The model has been validated against frontal and lateral, rigid impactor and sled experimental data [9-13]. However, the model lacks validation in the far-side loading mode, therefore, in order to use the GHBMC model in far-side related studies and to confirm the trustworthiness of its responses, it is inevitable to evaluate its impact response under far-side loading mode.

The objective of the current study was to evaluate the far-side impact response of the GHBMC HBM by comparing its various response parameters with PMHS experiments under 90-degree lateral, and 60-degree oblique impacts. In addition, rib fractures predicted by the HBM were also compared with those sustained by the PMHS.

II. METHODS

In order to evaluate the impact response of the restrained GHBMC model under far-side impact, the model was evaluated under two different impact scenarios - lateral (90 degree), and oblique (60 degree). Also simulations were performed with and without pre-tensioning in the seatbelt for each scenario. Experimental contact forces, regional accelerations and displacements were compared with simulations for both the scenarios. The correlation between the experimental and simulation data were quantified using correlation analysis (CORA). The rib fractures and corresponding AIS score observed in the experiments were compared with simulations.

Experimental Data Source

For completeness only a brief description of the experimental setup is presented in this work. A more detailed description can be found in Pintar, Yoganandan [8]. Five PMHS were tested under far-side (three lateral, and two oblique loading) using a sled system (Age: 79±7 years; height: 1.8±0.1 m; weight: 75±7 kg). A buck was mounted on the sled and the buck assembly included a standard configuration - center console and a three-point belt system. The center console was composed of a vertical pelvis plate, vertical leg plate, and a horizontal console plate. The pelvis and leg plates were designed to engage the respective anatomical regions of a 50th percentile male. The seatbelt system consisted of a low elongation webbing, and pre-tensioners and retractors were not used in the experiments. However, prior to the experiments, the PMHS were tightened until a belt pull length of 10 cm was achieved, to simulate a pre-tensioner. The same buck was used in both the lateral, and oblique impact scenarios by changing the orientation of the entire buck assembly. The load plates were instrumented with tri-axial load cells (three for the leg plate, two for the pelvis plate, and two for the center console plate). A VICON motion tracking system (1000 fps) was used to quantify the 3D kinematics of the PMHS that are attached with reflective markers. The markers were screwed into the bones at the head, T1, T12, and pelvis. Also, the PMHS were instrumented with tri-axial accelerometers at the T1 and T12. The head CG accelerations were derived using a pyramid nine accelerometer package (PNAP) [14]. The experimental data were normalized using equal stress equal velocity method to represent a 50^{th} percentile male [15,16].

Simulation Setup

A detailed finite element model of the experimental setup was constructed using various element types, and appropriate materials (Figure 1). The sled platform and components were not explicitly modeled in the simulation, however, the constraints associated with the sled system were mathematically implemented during the simulation. The rigid seat was constructed using shell elements and assigned steel material property that was used during contact and mass approximations. The backrest of the seat was also constructed using rigid shell elements, and attached to the seat frame using tied constraints. Rigid shell elements were used to construct a b-pillar that was used to anchor the shoulder belt. The dimensions of the load plates were directly taken from the experimental setup. Each load plate was constructed using two parts – a rigid plate, and paper honeycomb. The rigid plate on the load walls were made using shell elements and the paper honeycombs were constructed using solid elements. The honeycomb elements were assigned material properties corresponding to 208 kPa paper honeycombs. The thickness of the paper honeycomb was assigned 25 mm as observed in the experiments. Separate surface-to-surface contact interaction definitions were assigned between load plates and GHBMC body regions. A generic low-elongation three-point seatbelt system was used to restrain the GHBMC model. The anchor points of the system were selected to match experimental setup. The shoulder belt anchor

point was approximately 90 mm above and 120 mm behind the midpoint of the shoulder and in line with the end of the shoulder. The seatbelt system was made using shell and one dimensional elements. The belt region that interacted with the GHBMC model was created using shell elements, whereas the other regions were modeled using one dimensional elements. D-rings were modeled in appropriate places as observed in experiments.

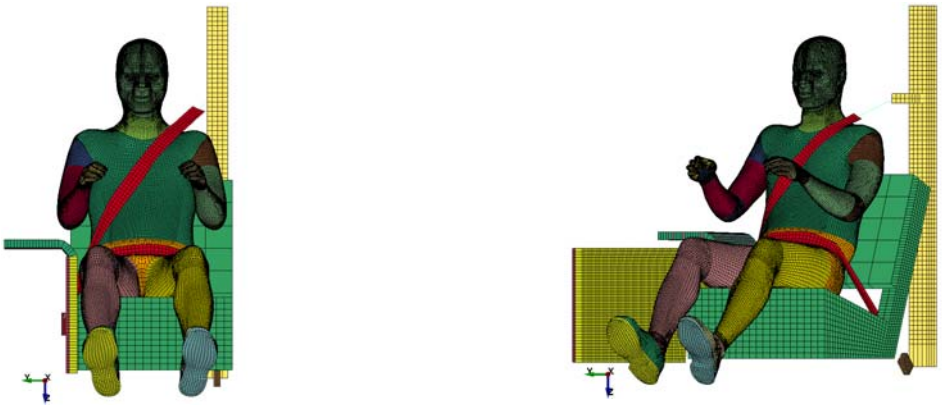

Figure 1 Pre-impact model setup of lateral and oblique scenarios

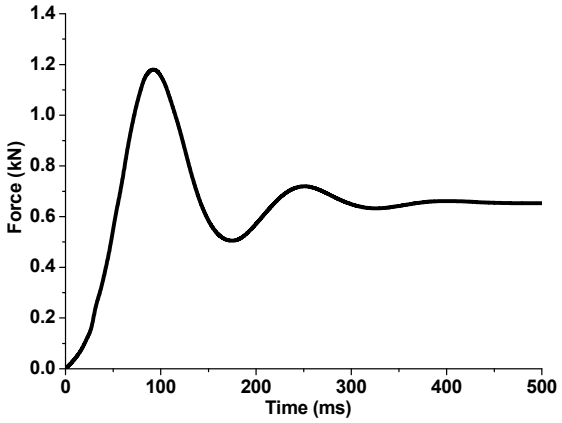

Figure 2 Contact force between the HBM and the seat model

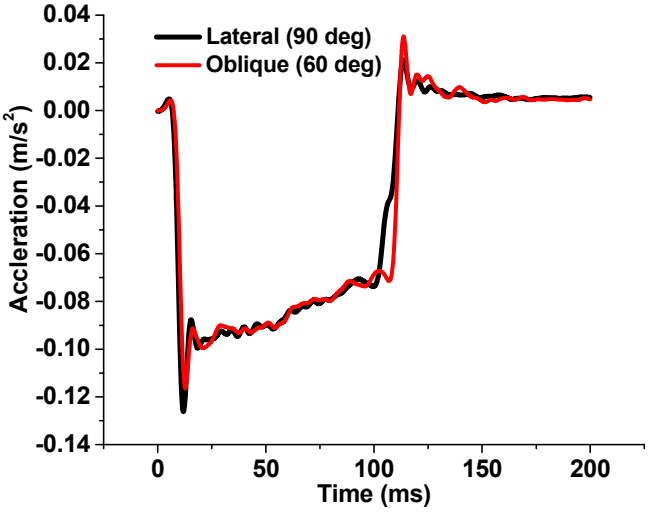

Figure 3 Acceleration pulse used in the lateral and oblique impacts

The GHBMC model was rotated and placed very close to the top of the seat and was settled on the seat using the acceleration due to gravity. To maintain the nominal posture, the spine and hands of the HBM were constrained during the gravity settling procedure. The contact force between the HBM and the seat model was monitored to confirm the absence of transient (Figure 2). The deformed geometry was then exported for restraint attachment. For the simulations without pre-tensioning, the seatbelt was snuggly fitted to the HBM. However, for the simulations with pre-tensioning, the seatbelt was pulled 10 cm in the negative x-direction using a predefined displacement. The deformed model was exported and the free-end of the seatbelt was attached to the B-pillar using tie constraint. The resultant contact forces were extracted from the pelvis, leg, and the console plates. Resultant nodal accelerations and y-axis displacements were extracted from the head CG, T1, T12, and sacrum. Rib fractures in the HBM were simulated using the element deletion option in LS-Dyna. The forces, accelerations, displacements, and the fractures were correlated with the experiments to quantify the biofidelity of the HBM under far-side impact mode. The severity of the fractures was classified using AIS score [17]. The rib cage was evaluated for fractures by using element elimination technique that used a plastic strain threshold value of 1.8%. Appropriate AIS scores were assigned based on the number of observed fractures in the rib cage. The lateral and oblique simulations were performed using the same buck model along with the HBM, however, the gross model was appropriately oriented to represent the impact scenario. Because of the presence of few direction dependent material properties that are defined with respect to a local coordinate system, the coordinates were rotated using affine transformations by utilizing a common origin. The entire buck model was given an initial velocity of 8.3 m/s using *INITIAL_VELOCITY keyword. The deceleration pulse from the experiments were directly applied to the seat using the *BOUNDARY_PRESCRIBED_MOTION LS-DYNA keyword (Figure 3). Visual comparison of the kinematics was performed between the simulation and experiment for the lateral impact using frames from anterior camera, however, anterior video of the PMHS was not available for the oblique impacts. To compare simulation and experimental responses, resultant nodal acceleration and load wall resultant contact force data from simulation results were compared with the normalized experimental data. All simulations were solved using LS-DYNA MPP version 7.0 solver on a Linux RHEL 5.4 computational cluster, using 64 cores. The principal directions and polarities followed in the current study are the same as those of the SAE J211 sign conventions.

Correlation and analyses (CORA) was used to quantify the goodness-of-fit between simulation and experimental responses. The ratings in CORA range from 0 to 1, where 0 representing poor correlation, and 1 representing perfect match. CORA uses two methods – that are fundamentally very different – to quantify the degree of correlations between the responses. The first method is the corridor method that calculates the correlation between the responses using user-defined corridors. This method calculates a mean trace using individual experimental responses. Along the mean trace, two corridors – an inner, and an outer corridor – are generated with a user defined constant y-offset. In this study, the inner corridors were calculated for 5 percent of the peak mean trace, whereas the outer corridor was calculated for 50 percent of the peak mean trace. For each time step, if the simulation response lies within the inner corridor then a rating of 1 is given, whereas if the response lies outside the outer corridor a rating of 0 is given. However, if the response lies in between the inner and the outer corridors a rating between 0 and 1 is given, based on the user defined blending function. The overall rating for the corridor method is calculated by averaging all ratings from each time step. The advantage of this method is its directness and simplicity; however, it tends to be sensitive to phase lag between responses. A cross-correlation method is used to compensate this disadvantage posed by the corridor method. The cross-correlation method is more involved and complex, for brevity, only a brief description is presented here, a more detailed description can be found in the literature [18]. This method quantifies the progression, time-shift, and size of the responses, using three respective metrics. The cross correlation method starts by time-shifting the mean curve by a small time step, and a cross correlation value is calculated for each time-shifted state. All the three metrics are calculated using the time-shifted data for the maximum cross correlation value. Weighted sum of these three metrics give the rating for correlation method. Equally weighted sum of the corridor, and cross-correlation methods give the overall correlation rating. The CORA parameters used in this study are listed in Table 1

Method	Parameters	Values	Description
Corridor	K	2	Transitional order of function between ratings of 1 and 0
	G_1	0.5	Weighting factor of the corridor method
	A_0	0.05	Width of the inner corridor
	B_0	0.5	Width of the outer corridor
	A_SIGMA	0	Parameter to widen the inner corridor
	B_SIGMA	0	Parameter to widen the outer corridor
Cross correlation	D_MIN	0.01	Minimum interval of evaluation
	D_MAX	0.12	Maximum interval of evaluation
	INT_MIN	0.8	Minimum interval overlap
	K_V	10	Transitional order of function between ratings of 1 and 0 for progression
	K_G	1	Transitional order of function between ratings of 1 and 0 for size
	K_P	1	Transitional order of function between ratings of 1 and 0 for phase
	G_V	0.5	Weighting factors of the progression rating
	G_G	0.25	Weighting factors of the size rating
	G_P	0.25	Weighting factors of the phase shift rating
	G_2	0.5	Weighting factors of the cross correlation method

Table 1 CORA parameters used in the current study

III. RESULTS

Each simulation took approximately 24 hours to solve on a high performance computing cluster. A visual comparison of the kinematics between experiment and simulation for with and without pre-tensioning cases were shown in Figure 4 and Figure 5, for the lateral and oblique impacts, respectively. Overall comparison showed a good agreement in both the impact modes for the case with pre-tensioning. However, in the case without pre-tensioning the results indicated poor seatbelt retention. In all the simulations, immediately after the buck started to decelerate the HBM continued to traverse laterally with its initial velocity. However, in the pre-tensioned cases, and in both the impacts, the seatbelt engaged the upper torso at the ipsilateral shoulder resulting in upper torso retention as observed in the experiments. In the impacts without pre-tensioning, the shoulder belt slipped tangentially to the sternum resulting the upper torso to rest on the center console plate. The displacements of the head CG, T1, T12, and sacrum with respect to the seat is shown in Figure 6 for the lateral and oblique impacts. In the lateral impact, the average head displacements in the experiments, with- and without pre-tensioned cases were 487, 436, and 575 mm respectively, whereas, the displacements at the T1, T12, and sacrum were 334, 243, and 376 mm; 116,136, and 192 mm; and 42, 74, and 94 mm respectively. In the oblique impact, the average head displacements were 536, 376, and 450 mm respectively, whereas, the displacements at the T1, T12, and sacrum were 395, 197, and 271 mm; 123,116, and 140 mm; and 38, 74, and 92 mm respectively.

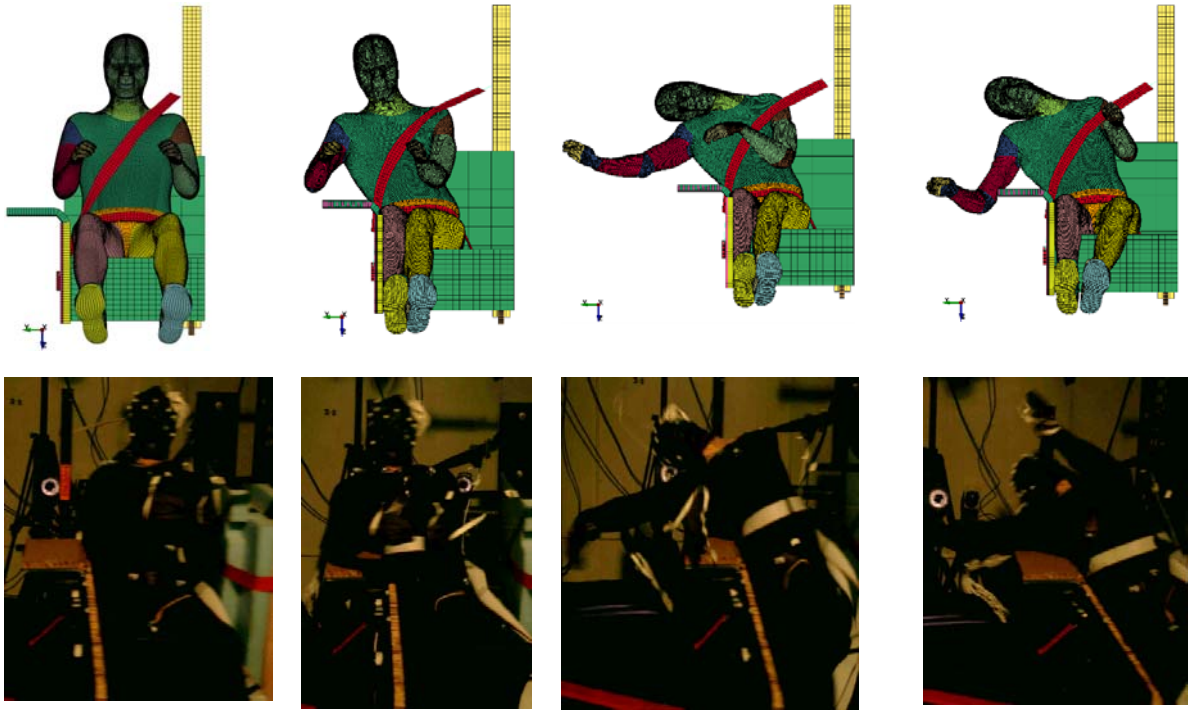

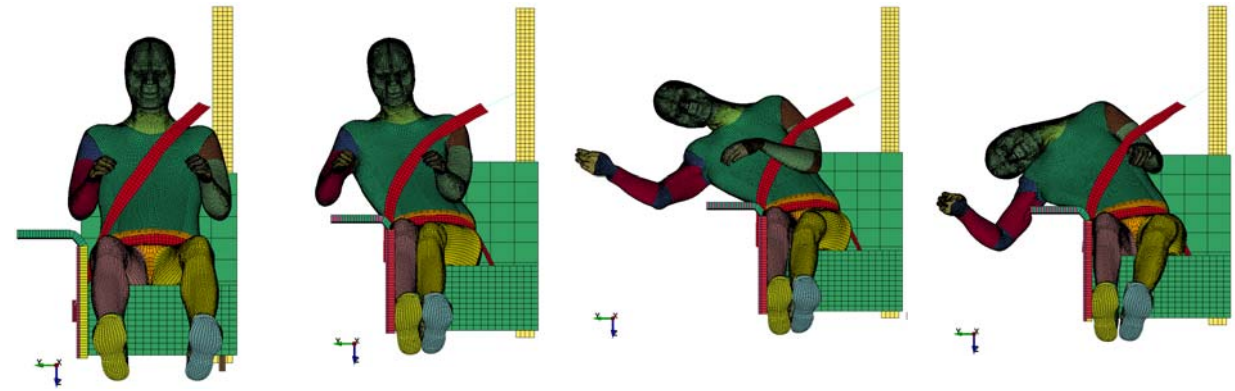

Figure 4 Visual kinematics comparison: simulated lateral impact with pre-tensioning (top row); experimental lateral impact with pre-tensioning (middle row); simulated lateral impact with no pre-tensioning (bottom row)

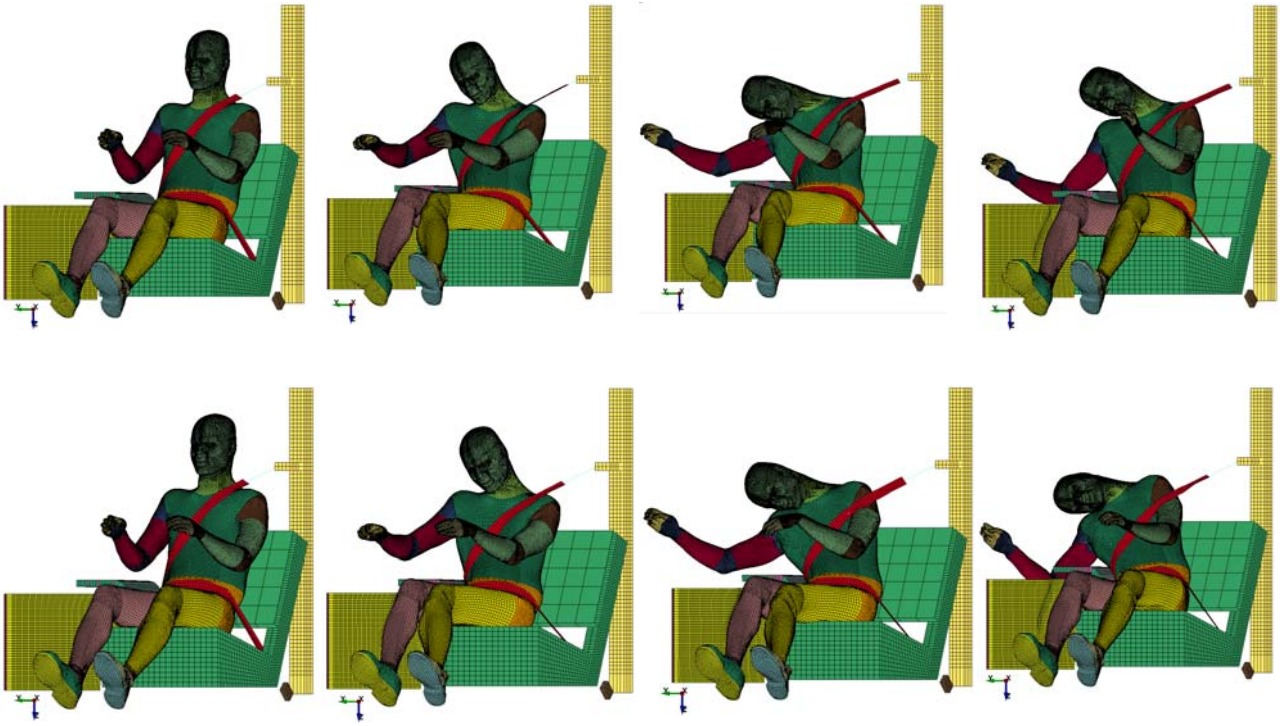

Figure 5 Visual kinematics comparison: simulated oblique impact with pre-tensioning (top row); simulated oblique impact with no pre-tensioning (bottom row)

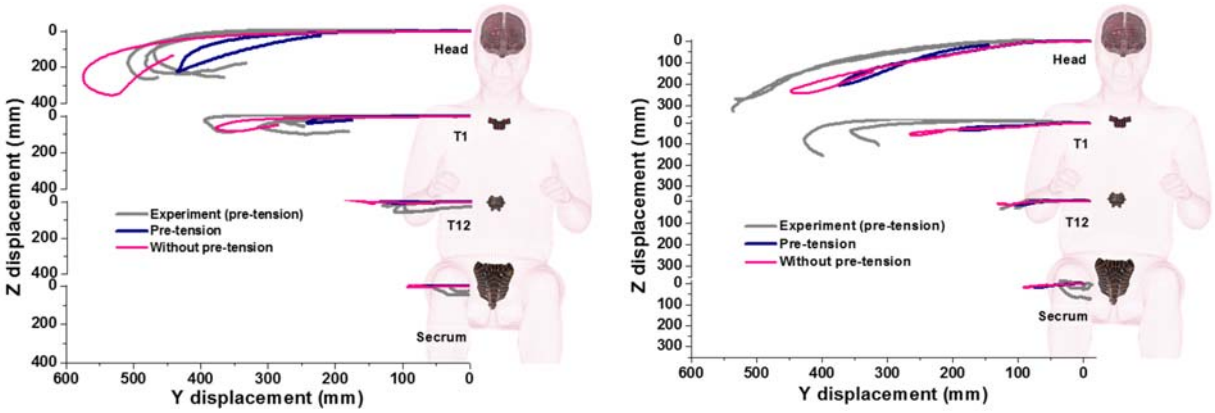

Figure 6 Regional displacements in the lateral (left), and oblique (right) impacts

The comparison of resultant accelerations between the HBM and PMHS for the with and without pre-tensioned cases are shown in Figure 7 and Figure 8 for the lateral and oblique impacts, respectively. The comparison of resultant regional contact forces between the HBM and PMHS for with and without pre-tension cases are shown in Figure 9 and Figure 10 for the lateral and oblique impacts, respectively. In the lateral impact, the resultant head, T1, and T12 accelerations in the experiments, with, and without pre-tension cases were 32±4, 32, and 33 g; 24±2, 24, and 20 g; and 20±5, 36, and 41 g respectively. Whereas, the resultant contact forces at the console, leg, and pelvis were 892±145, 1178, and 2001 N; 5548±975, 5385, 5368 N; and 5668±2404, 7082, and 8509 respectively. In the oblique impact, the resultant head, T1, and T12 accelerations in the experiments, with, and without pre-tension cases were 29±4, 24, and 18 g; 21±7, 21, and 22 g; and 19±2, 32, and 39 g respectively. Whereas, the resultant contact forces at the console, leg, and pelvis were 990±233, 621, and 1216 N; 4875±389, 4575, 4176 N; and 4086±534, 3492, and 4773 respectively. In the oblique impact, approximately 5 ms into the event a sharp increase in the T1 resultant accelerations were observed in both with and without pre-tensioning cases. In addition, in both the impacts, T12 resultant accelerations were over predicted by the HBM in both the pretension cases. In the contact forces, the cases without pre-tensioning consistently over predicted the forces with pre-tensioning in both the impact modes, with an exception to the leg contact force, in which the opposite was observed. The CORA ratings of the head, T1, T12 accelerations; and console, leg, and pelvis forces for the with and without pre-tension cases in the lateral case were 0.9 and 0.8, 0.8 and 0.7, 0.6 and 0.5; 0.5 and 0.3, 0.7 and 0.5, 0.7 and 0.6 respectively. The CORA ratings of the head, T1, T12 accelerations; and console, leg, and pelvis forces for the with- and without pre-tension cases in the oblique case were 0.7 and 0.6, 0.5 and 0.4, 0.5 and 0.4; 0.5 and 0.4, 0.6 and 0.4, 0.2 and 0.6 respectively. The CORA ratings were consistently higher in the pre-tensioned case compared to the case with no pre-tensioning in both the impact scenarios, with an exception to the pelvis force in the oblique impact in which the opposite was observed (Figure 11). The average combined CORA ratings for the with and without pre-tensioning cases were 0.7 and 0.56 in the lateral impact, and the ratings were 0.5 and 0.46 in the oblique impact (Figure 12).

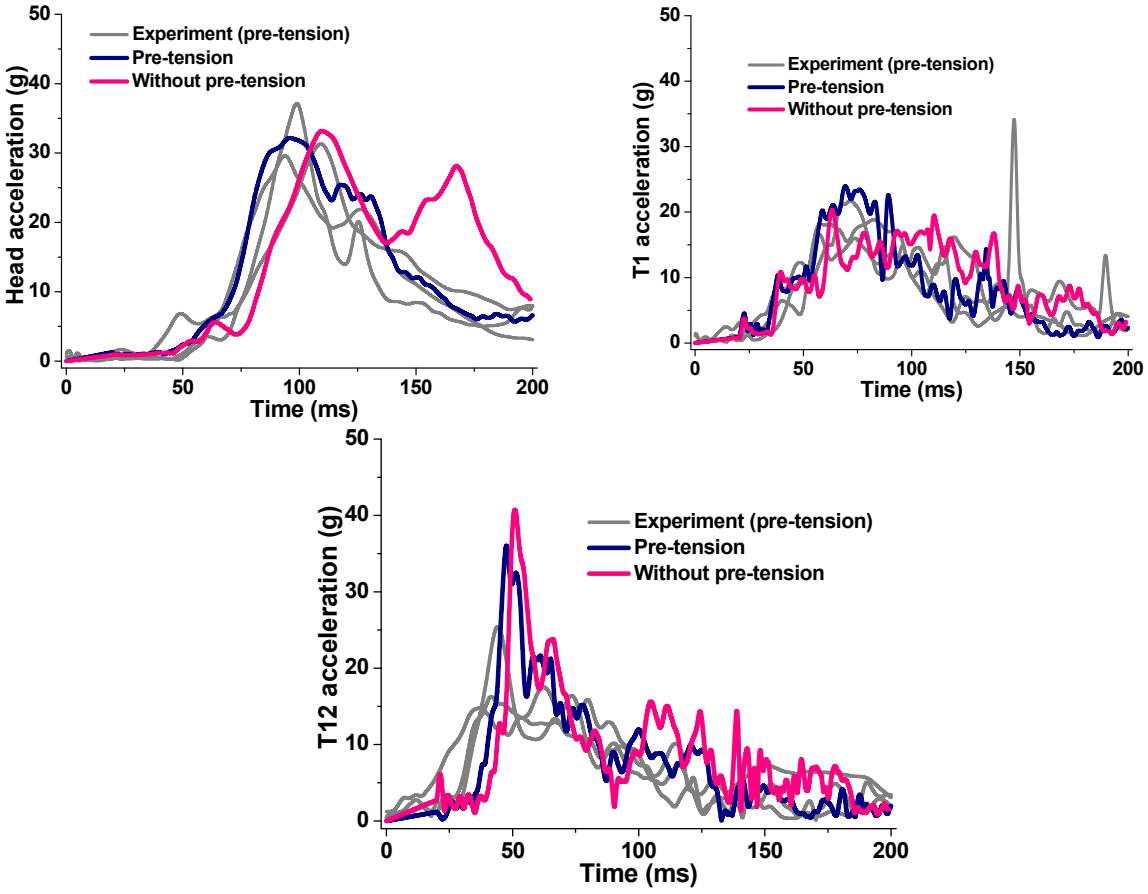

Figure 7 Regional resultant accelerations in the lateral impact

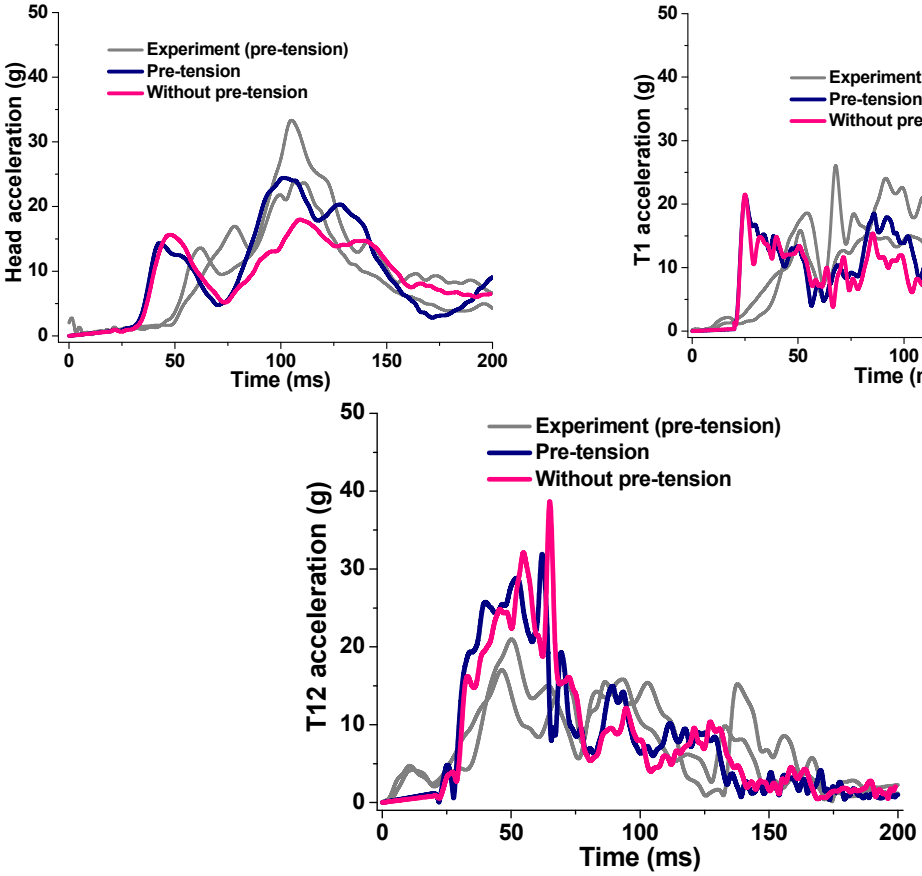

Figure 8 Regional resultant accelerations in the oblique impact

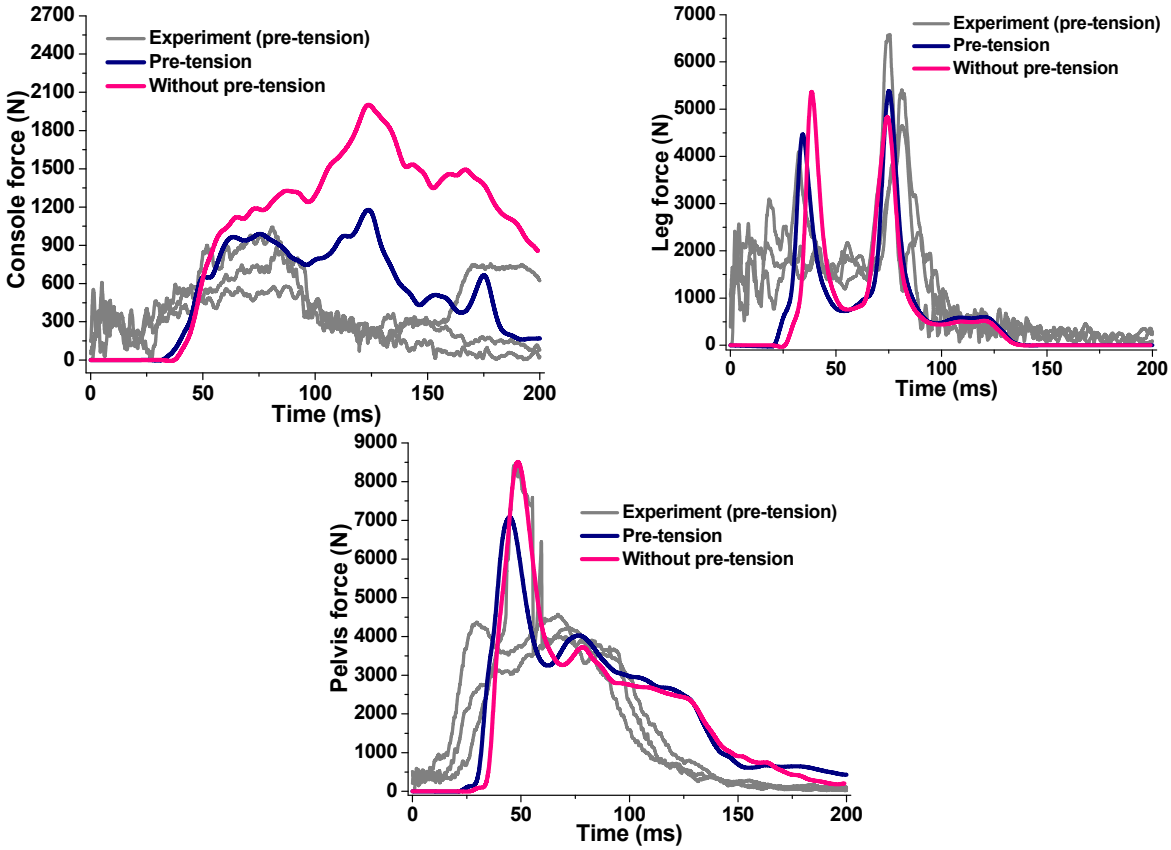

Figure 9 Regional contact forces in the lateral impact

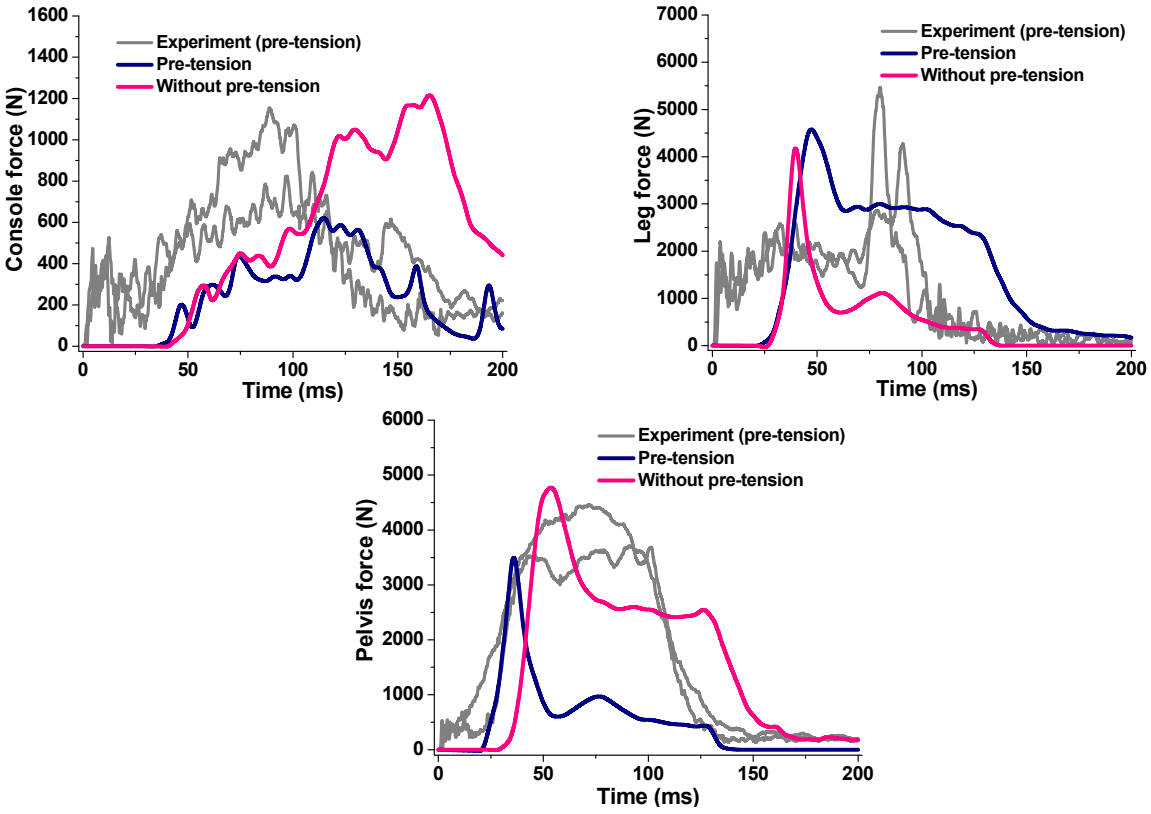

Figure 10 Regional contact forces in the oblique impact

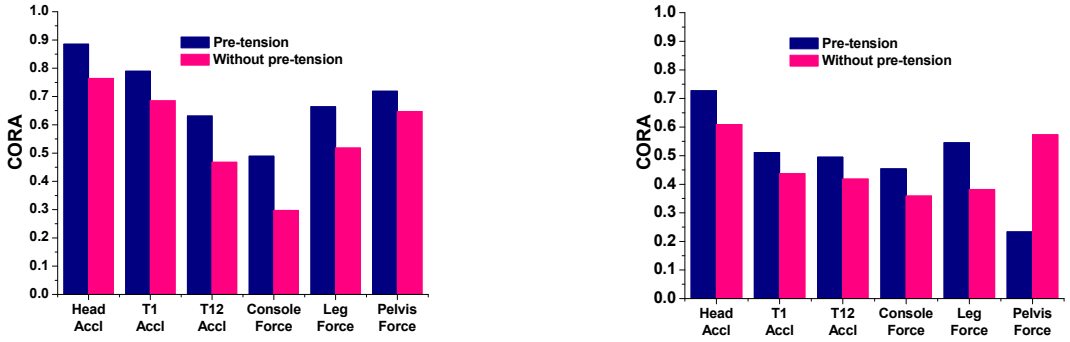

Figure 11 Regional CORA ratings in the lateral (left), and oblique (right) impacts

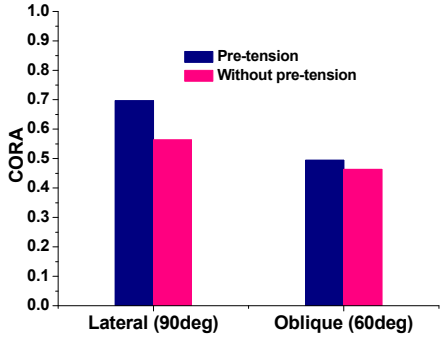

Figure 12 Average CORA ratings in the lateral, and oblique impacts

The comparison of the rib fractures in the lateral impact between the HBM and PMHS for the with and without pre-tensioned cases are shown in Figure 13. In the lateral impact, the PMHS sustained a total of six

fractures in which five of the fractures were on the right side (ribs 3,7,8,9) and one on the right (rib 7). The pre-tensioned HBM predicted three fractures, all on the right side (ribs 5,8,9), whereas, the HBM simulation without pre-tensioning predicted seven rib fractures - five on the right side (ribs 7,8,9,10) and two on the left (ribs 8,9). The comparison of the rib fractures between the HBM and PMHS for the with and without pre-tensioned cases are shown in Figure 14 for the oblique impacts. In the oblique impact, the PMHS sustained a total of six fractures all on the right side (ribs 3,4,5,6,7,8) and one on the right (rib 7). The pre-tensioned HBM predicted three fractures, all on the right side (ribs 6,7,8), whereas, the HBM simulation without pre-tensioning predicted four rib fractures - three on the right side (ribs 8,9,10) and two on the left (ribs 9). AIS scores in the experimental lateral and oblique impacts ranged from 2 to 5 and 3, whereas, the simulation estimated a score of 2 in both the impacts (Table 2). In summary, the simulations with the pre-tensioned HBM under-predicted the number of fractures as compared to the PMHS, and the HBM predicted fractures were higher in the cases with no pre-tensioning compared to those of with pre-tensioning. The average peak shoulder belt forces in the experiments, with and without pre-tensioning for the lateral and oblique cases were 2687, 2842, and 1736 N; and 3428, 3257, and 3026 N respectively.

Figure 13 Comparison of rib fractures between experiment (left) and simulation (right) in the lateral impact

Figure 14 Comparison of rib fractures between experiment (left) and simulation (right) in the oblique impact

Orientation	Belt presets	Number of rib fractures		AIS	
		Left side	Right side	Simulation	Experiment
Lateral	Pretension	3	0	2	2 to 5
	Without pretension	4	2	3	
Oblique	Pretension	3	0	2	3
	Without pretension	3	1	3	

Table 2 AIS grading of the rib fractures in experiments and simulations

IV. DISCUSSION

As indicated in the introduction, the objective of the current study was to evaluate the impact response of the GHBMC HBM by comparing various response parameters to those obtained from PMHS experiments. In addition, rib fractures predicted by the HBM were also compared with the PMHS. The simulated pre-tensioned cases under-predicted the head and T1 displacement compared to those of PMHS. A possible explanation of this might be the lateral bending stiffness of the whole spine may have played a key role in determining the head and T1 right lateral displacement. Higher spinal lateral joint stiffness of the spine could have resulted in under-

estimation of the regional displacements by the HBM. Because of the presence of the center console plate, the difference in displacements between the HBM and PMHS at T12 and sacrum were minimum. The poor seatbelt retention in the HBM simulations without pre-tensioning resulted in higher right lateral displacements at the head and T1 regions, compared to HBM cases with pre-tensioning. The pre-tensioning of the seatbelt increased the chances of shoulder belt retention by applying higher force on the ipsilateral shoulder compared to the cases without pre-tensioning. However, the pre-impact tensioning of the seatbelt in both the PMHS and HBM may not be equivalent to using a post-impact pyrotechnic pre-tensioner that are activated in real world crashes. Therefore, further studies are required to understand the equivalency of the two pre-tensioning mechanisms.

The resultant accelerations were over-estimated by the HBM at the T12 level in both the impact scenarios for both with and without pre-tensioning cases when compared to PMHS. The results reported in this study appear to support that the resilience of the rib cage is likely to have played a role in this over-estimation of accelerations. The regional higher stiffness at the rib cage may have caused the accelerations at the T12 level to abruptly increase upon impact against the center console plate. This rationale can also be extended to the pelvic region of the HBM. The pelvis plate contact force versus time trace extracted from the experiments indicated a flat region between the loading and unloading phase of the trace, indicating the resilience in the pelvic region of the PMHS. However, the pelvis contact force response in the HBM showed a rapid loading and unloading behavior that may indicate a higher pelvic regional stiffness compared to PMHS. The average CORA ratings were higher in the lateral impact compared to the oblique impact. There could be several possible explanations for this behavior, one could be the spine stiffness of the HBM in the anterio-right lateral direction may not be equivalent to that of a PMHS spine. Tuning the stiffness in this direction may improve the gross response of the HBM under oblique impact. Fundamentally, accurate spine stiffness in the anterio-posterior and in the lateral directions should result in a reasonable response in the other intermediate directions. In addition, the coupling of the internal organs among themselves and to the spine may have also contributed to this discrepancy. The CORA ratings for the non-pre-tensioned simulations were performed to reassure that pre-tensioned simulations were performed using realistic boundary and loading conditions mimicking the sled tests. Also, to highlight the significance of pre-tensioning by showing the difference in CORA ratings between with and without pre-tensioned cases. For example, in the lateral case, the pre-tensioned case showed an average CORA rating of 0.70, whereas, the non-pre-tensioned case showed 0.56, indicating the importance of pre-tensioning to obtain a realistic responses close to reference tests.

The HBM predicted a distinct pattern of rib fractures in the lateral impacts. Majority of the fractures were concentrated at the anterior region of the right lower quadrant of the rib cage indicating a combination of the belt loading and impact loading due to the contact with the center console plate. The fractures observed in the left side of the rib cage in the case with no pre-tensioning was likely due to the higher impact loading by the center console compared to the case with pre-tensioning. In the oblique impact, the HBM predicted fractures were distributed in the mid (in the anterio-posterior direction) right side region of the rib cage as observed in the experiments. This strongly correspond to the engagement of the shoulder belt with this region of the rib cage. In the lateral case, the webbing predominately engaged the right lower quadrant, whereas, in the oblique loading, the webbing engagement with the rib cage was more distributed along the mid right quadrant. The comparison of the rib fractures between the HBM and PMHS should be interpreted with caution as it is confounded by the quality of the rib cage material in the PMHS. The increased AIS ratings of rib fractures in the experiments may have attributed to the difference in the representative ages between the PMHS (average: 79 years), and HBM (26 years). Kent, Forman [19] performed lateral far-side impacts using PMHS seated on a sled system and reported a similar trend in rib fractures, however, the boundary conditions significantly differed from the current study due to the absence of the console, leg, and pelvis plates in their experimental setup. One of the key limitations of the current study was that only one speed was used in both the lateral and oblique impacts. To obtain a robust evaluation, response parameters of the HBM should be evaluated using experimental data with varied input velocities, if available. Also, the variations in the initial posture between the HBM and PMHS should be minimized for an improved evaluation. However, Park, Kim [11] reported that this difference in initial posture is likely to have a minimum influence on the response of the HBM under side impact.

V. CONCLUSIONS

The impact response of the GHBMC HBM was evaluated by comparing various response parameters (regional accelerations and contact forces) with PMHS experiments. In addition, rib fractures predicted by the HBM were also compared with those sustained by the PMHS. All the simulations with the pre-tensioned HBM under-predicted the number of fractures that are observed in the PMHS and the HBM predicted fractures were higher in the cases with no pre-tensioning compared to those of with pre-tensioning. In the pre-tensioned case, the HBM under-predicted the head and T1 displacements, whereas, over predicted T12 and sacrum in both the impact cases. The average combined CORA ratings of the accelerations and contact forces for the with and without pre-tensioning cases were 0.7 and 0.56 in the lateral impact, and the ratings were only 0.5 and 0.46 in the oblique impact. In summary, the study recommends further improvement in the biofidelity of the model under oblique loading mode by improving the biofidelity at the core component level – thoracic and lumbar spine for example.

VI. ACKNOWLEDGEMENT

The study was supported by the US Department of Transportation DTNH22-13-D-00290. This material is the result of work supported with resources and the use of facilities at the Zablocki VA Medical Center, Milwaukee, Wisconsin and the Medical College of Wisconsin. The authors would like to thank the Global Human Body Model Consortium for providing the model for this study. The authors would also like to thank Argonne National Laboratory for providing cluster resources. Any views expressed in this article are those of the authors and not necessarily representative of the funding organizations.

VII. REFERENCES

[1] Augenstein, J., Perdeck, E., et al. Injuries to restrained occupants in far-side crashes. *Annual proceedings / Association for the Advancement of Automotive Medicine. Association for the Advancement of Automotive Medicine*, 2000. 44: p. 57-66

[2] Digges, K. and Dalmotas, D. Injuries to Restrained Occupants in Far-Side Crashes, in *ESV*. 2001.

[3] Digges, K. and Dalmotas, D. Injuries to restrained occupants in far-side crashes. *Spine*, 2004. 7(5): p. 16

[4] Digges, K., Gabler, H., Mohan, P., and Alonso, B. Characteristics of the injury environment in far-side crashes. *Annual proceedings / Association for the Advancement of Automotive Medicine. Association for the Advancement of Automotive Medicine*, 2005. 49: p. 185-97

[5] Fildes, B., Fitzharris, M., Gabler, H.C., Digges, K., and Smith, S. Chest and abdominal injuries to occupants in far side crashes. *Proceedings of The 20th International Technical Conference on Enhanced Safety of Vehicles (ESV) Proceedings–Lyon, France, June 18-21, Paper No. 07-0384-O*, 2007.

[6] Halloway, D.E. Occupant Kinematics in Distinct Types of Far-side Impacts. 2016, SAE Technical Paper.

[7] Forman, J.L., Lopez-Valdes, F., et al. Occupant kinematics and shoulder belt retention in far-side lateral and oblique collisions: a parametric study. *Stapp car crash journal*, 2013. 57: p. 343

[8] Pintar, F.A., Yoganandan, N., et al. Comparison of PMHS, WorldSID, and THOR-NT responses in simulated far side impact. *Stapp car crash journal*, 2007. 51: p. 313-60

[9] Hayes, A.R., Vavalle, N.A., Moreno, D.P., Stitzel, J.D., and Gayzik, F.S. Validation of simulated chestband data in frontal and lateral loading using a human body finite element model. *Traffic injury prevention*, 2014. 15(2): p. 181-6

[10] Park, G., Kim, T., Crandall, J.R., Arregui Dalmases, C., and Luzón Narro, B.J. Comparison of kinematics of GHBMC to PMHS on the side impact condition. *Proceedings of 2013 IRCOBI Conference Proceedings*, 2013.

[11] Park, G., Kim, T., et al. Evaluation of Biofidelity of Finite Element 50th Percentile Male Human Body Model (GHBMC) under Lateral Shoulder Impact Conditions, in *IRCOBI*. 2014: Berlin.

[12] Vavalle, N.A., Davis, M.L., Stitzel, J.D., and Gayzik, F.S. Quantitative Validation of a Human Body Finite Element Model Using Rigid Body Impacts. *Annals of biomedical engineering*, 2015

[13] Arun, M.W.J., Humm, J.R., Yoganandan, N., and Pintar, F.A. Biofidelity Evaluation of a Restrained Whole Body Finite Element Model under Frontal Impact using Kinematics Data from PMHS Sled Tests, in *2015 IRCOBI Conference*. International Research Council on Biomechanics of Injury: Lyon , France. p. 622-633.

[14] Yoganandan, N., Humm, J., Schlick, M., and Pintar, F. Head motions using nine accelerometer package and angular rate sensors. *Biomedical sciences instrumentation*, 2007. 44: p. 256-261

[15] Eppinger, R.H. Prediction of thoracic injury using measurable experimental parameters. *Proceedings of Proceedings of the International Conference of Experimental Safety Vehicles, NHTSA, Washington, DC*, 1976.

[16] Yoganandan, N., Arun, M.W., and Pintar, F.A. Normalizing and scaling of data to derive human response corridors from impact tests. *Journal of biomechanics*, 2014. 47(8): p. 1749-56

[17] Gennarelli, T.A. and Wodzin, E. AIS 2005: a contemporary injury scale. *Injury*, 2006. 37(12): p. 1083-1091

[18] Gehre, C., Gades, H., and Wernicke, P. Objective rating of signals using test and simulation responses. *Proceedings of 21st International Technical Conference on the Enhanced Safety of Vehicles, Stuttgart, Germany*, 2009.
[19] Kent, R., Forman, J., Lessley, D., Arbogast, K., and Higuchi, K. A parametric study of far-side restraint mechanics. *Proceedings of Proc. Conference on the Enhanced Safety of Vehicles Paper*, 2013.